Fractional cable equation for general geometry: A model of axons with swellings and anomalous diffusion

Erick J. López-Sánchez*
Posgrado en Ciencias Naturales e Ingeniería, Universidad Autónoma Metropolitana, Cuajimalpa and Vasco de Quiroga 4871, Santa Fe Cuajimalpa, Ciudad de México 05300, Mexico

Juan M. Romero†
Departamento de Matemáticas Aplicadas y Sistemas, Universidad Autónoma Metropolitana-Cuajimalpa, Vasco de Quiroga 4871, Santa Fe Cuajimalpa, Ciudad de México 05300, Mexico

Huitzilin Yépez-Martínez‡
Universidad Autónoma de la Ciudad de México, Prolongación San Isidro 151, San Lorenzo Tezonco, Iztapalapa, Ciudad de México 09790, Mexico

(Received 5 June 2017; revised manuscript received 30 August 2017; published 20 September 2017)

Different experimental studies have reported anomalous diffusion in brain tissues and notably this anomalous diffusion is expressed through fractional derivatives. Axons are important to understand neurodegenerative diseases such as multiple sclerosis, Alzheimer's disease, and Parkinson's disease. Indeed, abnormal accumulation of proteins and organelles in axons is a hallmark of these diseases. The diffusion in the axons can become anomalous as a result of this abnormality. In this case the voltage propagation in axons is affected. Another hallmark of different neurodegenerative diseases is given by discrete swellings along the axon. In order to model the voltage propagation in axons with anomalous diffusion and swellings, in this paper we propose a fractional cable equation for a general geometry. This generalized equation depends on fractional parameters and geometric quantities such as the curvature and torsion of the cable. For a cable with a constant radius we show that the voltage decreases when the fractional effect increases. In cables with swellings we find that when the fractional effect or the swelling radius increases, the voltage decreases. Similar behavior is obtained when the number of swellings and the fractional effect increase. Moreover, we find that when the radius swelling (or the number of swellings) and the fractional effect increase at the same time, the voltage dramatically decreases.

DOI: 10.1103/PhysRevE.96.032411

I. INTRODUCTION

In biological organisms there are hydrogen atoms in abundance, particularly in water and fat. These atoms allow us to study biological organisms with noninvasive techniques, such as magnetic resonance imaging (MRI). Indeed, using a magnetic field and the Zeeman effect, the diffusion process of water molecules in biological tissues can be mapped [1,2]. Thus, using these techniques, it is possible to study some physiological properties of biological tissues, for example, water molecule diffusion patterns can reveal microscopic details about tissue architecture and can reflect interactions with many obstacles, such as macromolecules, fibers, and membranes [1–4]. Notably, in neuroscience water diffusion can provide information about white matter integrity, fiber density, uniformity of nerve fiber direction, axonal membranes, cytoskeleton properties, etc. [3,4]. In fact, water diffusion has been used to detect and characterize different neurodegenerative diseases [5]. For instance, using diffusion tensor imaging (DTI), altered diffusion has been detected in white matter of subjects with multiple sclerosis [6–8]. Also, using DTI, white matter alterations were found in the corpus callosum of subjects with Huntington's disease [9]. Moreover, using DTI, relevant white matter abnormalities were found in Alzheimer's disease [10,11]. In addition, using MRI, hippocampal atrophy has been detected in Parkinson's disease [12]. Even more, different experimental studies have shown that water diffusion in some tissues cannot be described by a Gaussian model, but as an anomalous diffusion expressed through fractional calculus [13–18], in particular in brain tumors [19–21] and dendrites [22]. Furthermore, some authors have suggested that the anomalous diffusion parameters might play a role in the diagnosis of brain diseases [23]. It is worth mentioning that in different neurodegenerative diseases abnormal accumulations of proteins and organelles are reported that disrupt axonal transport [24–26]. Additionally, different theoretical studies support the claim that anomalous diffusion appears in a heterogeneous medium [27–29]. For these reasons, diffusion and anomalous diffusion in brain tissues are relevant in the study of the brain physiology. Other studies about anomalous diffusion in cellular systems can be seen in Refs. [30–33].

Another aspect essential to understanding how the brain works is given by its electrical activity. Thus, in order to obtain a reasonable model of the brain, it is important to know how the voltage propagates in brain tissues with anomalous diffusion. In particular, because axons are crucial in neuron-to-neuron communications and can be described as cables, we should know how the voltage propagates in a cable with anomalous diffusion. In this respect, to study the voltage $V(x,t)$ in a straight cylindrical cable with a circular cross section of constant diameter d_0 and anomalous diffusion, recently several

*lsej@unam.mx
†jromero@correo.cua.uam.mx
‡huitzilin.yepez.martinez@uacm.edu.mx

authors have proposed a fractional cable equation [34,35]

$$c_M \frac{\partial V(x,t)}{\partial t} = \beta_\nu D_{\nu t}\left(\frac{d_0}{4r_L}\frac{\partial^2 V(x,t)}{\partial x^2} - i_{\text{ion}}\right), \tag{1}$$

where c_M denotes the specific membrane capacitance, r_L denotes the longitudinal resistance, i_{ion} is the ionic current per unit area into and out of the cable,

$$D_{\nu t} = \frac{\partial^{1-\nu}}{\partial t^{1-\nu}}, \quad \nu = \text{const}, \quad 0 \leqslant \nu \leqslant 1, \tag{2}$$

is the Riemann-Liouville fractional operator [36], and β_ν is a constant with $(\text{time})^{1-\nu}$ dimensions. The passive cable case, namely, when $i_{\text{ion}} = V/r_M$ (where r_M is the specific membrane resistance), was used to study electrodiffusion of ions in nerve cells [34,35].

Additionally, there are different physiological phenomena where the geometry is important. For instance, axons with nontrivial geometry are important to the understanding of some neurodegenerative diseases; indeed, discrete swellings along the axons appear in neurodegenerative diseases such as Alzheimer's disease, Parkinson's disease, HIV-associated dementia, and multiple sclerosis. In fact, axons with a diameter of approximately 1 μm with a swelling with a diameter of approximately 5 μm are reported in Parkinson's disease [37]. In addition, axons with a diameter of approximately 4 μm with a swelling with a diameter of approximately 60 μm are reported in multiple sclerosis [38]; axons with a diameter of approximately 1.5 μm with a swelling train, where the swelling diameter varies between 4 and 10 μm, are reported in Alzheimer's disease [39–41]; axons with a diameter of approximately 6 μm and swellings with a diameter of approximately 43 μm are reported in HIV-associated dementia [42–46]. Other sizes of the axonal swellings can be see in Refs. [47,48]. Some theoretical studies on cables with noncylindrical geometry can be seen in Refs. [49–56]. Because Eq. (1) only describes axons with cylindrical geometry, in order to study the voltage propagation in a cable with nontrivial geometry and anomalous diffusion, this equation should be generalized.

In this paper we study the voltage propagation in a cable with anomalous diffusion and nontrivial geometry. For this purpose, we introduce a fractional cable equation for a general geometry. This generalized equation depends on fractional parameters β_ν and ν and geometric quantities such as the curvature and torsion of the cable. For different cable geometries, we show that in modeling a system where the voltage decreases, we should suppose that β_ν increases when ν decreases. For a straight cylinder with a constant radius we show that the voltage depends on neither the curvature nor the torsion of the cable and it decreases when β_ν increases and ν decreases. In addition, cables with swellings are studied. In these last cable geometries we find that when the swelling radius increases or β_ν increases and ν decreases, the voltage decreases dramatically.

This paper is organized as follows. In Sec. II we propose a fractional cable equation with a general geometry. In Sec. III we analyze some general properties of the generalized fractional cable equation. In Sec. IV we consider the cylindrical cable with a constant radius. In Sec. V we study a cable with swellings. In Sec. VI a summary is given.

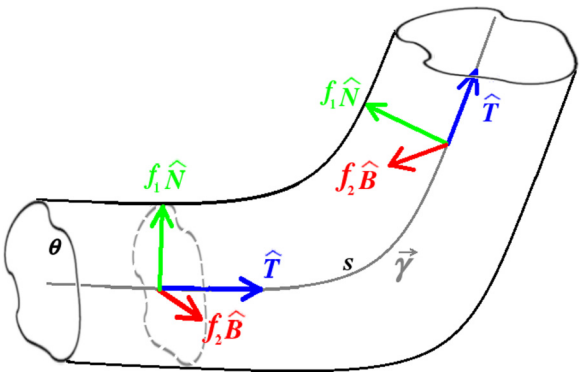

FIG. 1. Cable with a general geometry. The vectors $\hat{T}$, $\hat{N}$, and $\hat{B}$ are shown at two different points on the curve $\vec{\gamma}$.

II. FRACTIONAL CABLE EQUATION IN A GENERAL GEOMETRY

It is well known that to study the geometric properties of a three-dimensional curve $\vec{\gamma}$ the arc length parameter

$$s = \int_0^x \sqrt{\frac{d\vec{\gamma}(\zeta)}{d\zeta}\cdot\frac{d\vec{\gamma}(\zeta)}{d\zeta}}\,d\zeta \tag{3}$$

is a friendly parameter. Indeed, using the arc length parameter (3), we can construct the vectors of the Frenet-Serret frame [57]

$$\frac{d\vec{\gamma}(s)}{ds} = \hat{T}, \quad \hat{N} = \frac{\frac{d\hat{T}}{ds}}{\left|\frac{d\hat{T}}{ds}\right|}, \quad \hat{B} = \hat{T}\times\hat{N}, \tag{4}$$

where $\hat{T}$ is the unit vector tangent, $\hat{N}$ is the normal unit vector, and $\hat{B}$ is the binormal unit vector to the curve. Furthermore, using the arc length and the Frenet-Serret frame, the Frenet-Serret formulas can be obtained as [57]

$$\frac{d\hat{T}}{ds} = \kappa\hat{N}, \quad \frac{d\hat{N}}{ds} = -\kappa\hat{T} + \tau\hat{B}, \quad \frac{d\hat{B}}{ds} = -\tau\hat{N}, \tag{5}$$

where κ and τ are the curvature and torsion of the curve $\vec{\gamma}$, respectively.

We can employ the Frenet-Serret frame to construct a cable model. Actually, we can propose a general cable as the region bounded by the surface

$$\vec{\Sigma}(\theta,s) = \vec{\gamma}(s) + f_1(\theta,s)\hat{N}(s) + f_2(\theta,s)\hat{B}(s), \tag{6}$$

where θ is an angular variable. Notice that employing the angular coordinate θ, the functions $f_1(\theta,s)$ and $f_2(\theta,s)$, and the vectors $\hat{N}(s)$ and $\hat{B}(s)$, we are constructing the cable over the curve $\vec{\gamma}(s)$. In Fig. 1 we can see a representation of the surface (6). For instance, a cable with a deformed circular cross section, where the radius R depends on the angle θ, can be described by the surface (6), where

$$f_1(\theta,s) = R(\theta,s)\cos\theta, \quad f_2(\theta,s) = R(\theta,s)\sin\theta. \tag{7}$$

Notice that in this case the cross-section area is given by

$$a(s) = \frac{1}{2}\int_0^{2\pi} R^2(\theta,s)d\theta. \tag{8}$$

Some geometric quantities as the area of a surface can be written in terms of the first fundamental form, which is

constructed with the inner product on the tangent space of a surface as [57]

$$g = \begin{pmatrix} E & F \\ F & G \end{pmatrix}, \tag{9}$$

where

$$E = \frac{\partial \vec{\Sigma}(\theta,s)}{\partial s} \cdot \frac{\partial \vec{\Sigma}(\theta,s)}{\partial s}, \tag{10}$$

$$G = \frac{\partial \vec{\Sigma}(\theta,s)}{\partial \theta} \cdot \frac{\partial \vec{\Sigma}(\theta,s)}{\partial \theta}, \tag{11}$$

$$F = \frac{\partial \vec{\Sigma}(\theta,s)}{\partial s} \cdot \frac{\partial \vec{\Sigma}(s,\theta)}{\partial \theta}. \tag{12}$$

Now, let us remember that the curvature $\kappa(s)$ at a point P of the curve $\vec{\gamma}(s)$ is defined as the inverse of the radius of the osculating circle at P (see Ref. [58]). Then, if the radius of the osculating circle is small, the surface (6) describes a cable with a big curvature. In addition, notice that when the radius of the osculating circle is smaller than the radius of the cable, the cable surface touches itself. Axons with big curvature have not been reported in the literature. In this paper we suppose that at each point of the curve $\vec{\gamma}(s)$ the radius of the osculating circle is larger than the radius of the cable. Namely, at each point of the curve $\vec{\gamma}(s)$ we suppose that the curvature $\kappa(s)$ is smaller than $R^{-1}(s)$ and the inequality

$$\kappa(s)R(s) < 1 \tag{13}$$

is satisfied.

The axon geometry is important for diverse physiological processes such as voltage propagation. In this respect, according to Ref. [56], when the cable geometry is given by (6) the cable equation is

$$\frac{\partial V(s,t)}{\partial t} = \frac{1}{r_L c_M \int_0^{2\pi} d\theta \sqrt{\det g(\theta,s)}} \frac{\partial}{\partial s}\left(a(s)\frac{\partial V(s,t)}{\partial s}\right) - \frac{i_{\text{ion}}}{c_M}, \tag{14}$$

where $a(s)$ is the cable cross section and

$$\sqrt{\det g(\theta,s)} = \left\{ R^2(\theta,s)\left(\frac{\partial R(\theta,s)}{\partial s} - \tau \frac{\partial R(\theta,s)}{\partial \theta}\right)^2 + [1-\kappa(s)R(\theta,s)\cos\theta]^2\left[R^2(\theta,s) + \left(\frac{\partial R(\theta,s)}{\partial \theta}\right)^2\right]\right\}^{1/2}. \tag{15}$$

Notice that Eq. (14) depends on geometric quantities such as the curvature κ and torsion τ of the cable.

Then, in order to study the voltage propagation in a cable with general geometry and anomalous diffusion, we can employ Eqs. (1) and (14) to propose a generalized fractional cable equation

$$\frac{\partial V(s,t)}{\partial t} = \beta_\nu D_{\nu t}\left[\frac{1}{r_L c_M \int_0^{2\pi} d\theta \sqrt{\det g(\theta,s)}} \frac{\partial}{\partial s} \times \left(a(s)\frac{\partial V(s,t)}{\partial s}\right) - \frac{i_{\text{ion}}}{c_M}\right], \tag{16}$$

where

$$D_{\nu t} = \frac{\partial^{1-\nu}}{\partial t^{1-\nu}}, \quad \nu = \text{const}, \quad 0 \leqslant \nu \leqslant 1, \tag{17}$$

is the Riemann-Liouville fractional operator [36] and β_ν is a constant with $(\text{time})^{1-\nu}$ dimensions. The voltage in an infinite cable has to satisfy the Dirichlet boundary condition and a finite cable has to satisfy the Neumann boundary condition [59,60]; the solutions of Eq. (16) should satisfy these boundary conditions.

In the general case, i_{ion} depends on the voltage and Eq. (14) is a nonlinear differential equation. However, in the passive cable model we can take

$$i_{\text{ion}} = \frac{V(s,t)}{r_M}. \tag{18}$$

Therefore, the fractional cable equation for the passive cable model with the geometry given by (6) is

$$\frac{\partial V(s,t)}{\partial t} = \beta_\nu D_{\nu t}\left[\frac{1}{r_L c_M \int_0^{2\pi} d\theta \sqrt{\det g(\theta,s)}} \frac{\partial}{\partial s} \times \left(a(s)\frac{\partial V(s,t)}{\partial s}\right) - \frac{V(s,t)}{r_M c_M}\right]. \tag{19}$$

In the following sections we will study some solutions of this equation.

III. QUALITATIVE ANALYSIS

For a nontrivial geometry, finding solutions of Eq. (19) is a difficult task. However, let us provide a qualitative analysis of this equation. In this respect, we propose the voltage

$$V(s,t) = \mathcal{T}(t)X(s). \tag{20}$$

In this case Eq. (19) implies

$$\frac{1}{r_L c_M \int_0^{2\pi} d\theta \sqrt{\det g(\theta,s)}} \frac{\partial}{\partial s}\left(a(s)\frac{\partial X(s)}{\partial s}\right) - \frac{X(s)}{r_M c_M} = -\lambda X(s), \tag{21}$$

$$\frac{\partial \mathcal{T}(t)}{\partial t} = -\lambda \beta_\nu D_{\nu t}\mathcal{T}(t), \tag{22}$$

where λ is a constant. Moreover, if we take

$$X(s) = \frac{\psi(s)}{\sqrt{a(s)}}, \tag{23}$$

the spatial equation (21) can be written as

$$-\frac{\partial^2 \psi(s)}{\partial s^2} + U(s)\psi(s) = 0, \tag{24}$$

where

$$U(s) = \frac{r_L c_M \int_0^{2\pi} d\theta \sqrt{\det g(\theta,s)}}{a(s)}\left(\lambda - \frac{1}{r_M c_M}\right) - \frac{1}{2}\left(\frac{\left(\frac{da(s)}{ds}\right)^2}{2a^2(s)} - \frac{\frac{d^2a(s)}{ds^2}}{a(s)}\right). \tag{25}$$

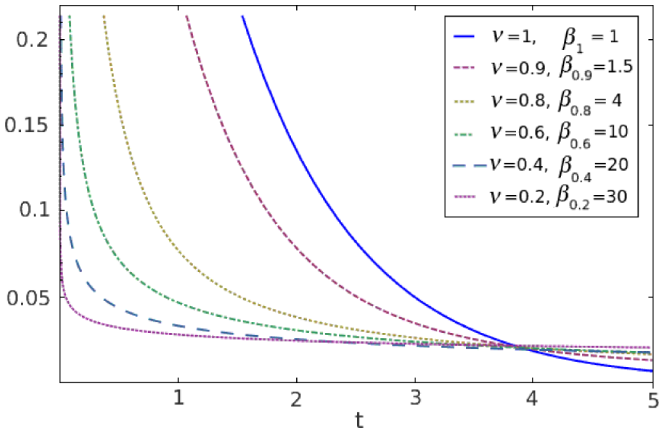

FIG. 2. Mittag-Leffler function for different values of β_ν and ν.

Observe that the parameters ν and β_ν do not appear in this equation. In fact, this spatial equation is the same spatial equation that appears in the nonfractional case [56]. In addition, observe that the parameter λ does not depend on ν or β_ν.

Furthermore, the Laplace transform of the temporal equation (22) implies

$$\tilde{\mathcal{T}}_\nu(\zeta) = \mathcal{T}(0)\frac{\zeta^{\nu-1}}{\zeta^\nu + \beta_\nu\lambda}, \tag{26}$$

where $\tilde{\mathcal{T}}_\nu(\zeta)$ is the Laplace transform of the function $\mathcal{T}_\nu(t)$. The inverse Laplace transform of the function (26) is given by [36]

$$\mathcal{T}_\nu(t) = \mathcal{T}(0)E_{\nu,1}(-\beta_\nu\lambda t^\nu), \tag{27}$$

where

$$E_{\nu,\Lambda}(z) = \sum_{n\geqslant 0}\frac{z^n}{\Gamma(\nu n + \Lambda)} \tag{28}$$

is the Mittag-Leffler-type function [36]. Notice that if $\nu = 1$ we obtain the usual solution

$$\mathcal{T}_1(t) = \mathcal{T}(0)e^{-\lambda t}. \tag{29}$$

In addition, if $\nu = 0$ we obtain

$$\mathcal{T}_0(t) = \mathcal{T}(0)\sum_{n\geqslant 0}(-\lambda\beta_0)^n, \tag{30}$$

TABLE I. Number of points n_s and n_t and time of the refinement.

Refinement	n_s	n_t
first time	1024	100
second time	2048	500
third time	4096	2000

which is a constant. We can observe that Eq. (30) only makes sense if

$$\beta_0\lambda < 1. \tag{31}$$

In this case we get

$$\mathcal{T}_0(t) = \frac{\mathcal{T}(0)}{1+\beta_0\lambda}. \tag{32}$$

In Sec. IV we saw that, for realistic parameters of the cylindrical cable, λ is the order of 10^{-3} $(\text{sec})^{-1}$. Then the inequality (31) is satisfied if β_0 is smaller than 10^3 sec.

Notice that the strongest fractional effect is obtained when ν is close to zero and in this case the function $\mathcal{T}_\nu(t)$ is close to the constant (32), which decreases when β_0 increases. Then, in order to model a system where the voltage decreases, we should take β_0 bigger than one, but satisfying the inequality (31). If we take β_0 close to zero, the voltage does not decrease.

Now recall that the usual case is obtained with $\nu = 1$ and $\beta_1 = 1$. Additionally, when ν is close to zero, β_ν should reach its maximum value; in fact, β_0 should be bigger than one. Thus, for a system where the voltage decreases, we can suppose that β_ν increases when ν decreases.

Figure 2 shows the function (27) for different β_ν and ν values. In this we can see that the function (27) decreases when β_ν increases and ν decreases.

Then, using the functions (27) and (23), we found the voltage

$$V(s,t) = \frac{\mathcal{T}(0)}{\sqrt{a(s)}}E_{\nu,1}(-\beta_\nu\lambda t^\nu)\psi(s), \tag{33}$$

where the function $\psi(s)$ satisfies Eq. (24). From Eq. (33) we can see that when the cable cross-sectional area $a(s)$ increases the voltage decreases. In addition, when β_ν increases and ν decreases the voltage decreases. Therefore, this qualitative analysis suggests that in an axon with transport or geometrical defects the voltage decreases.

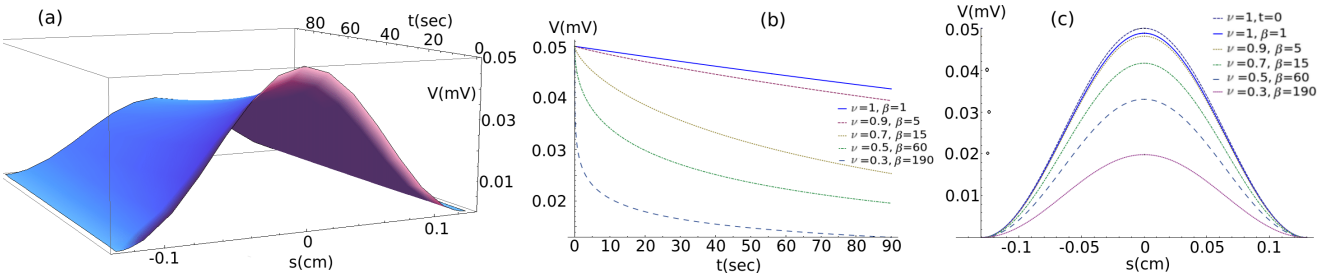

FIG. 3. (a) Voltage for the cylindrical cable for $\nu = 0.7$ and $\beta_{0.7} = 15$ $(\text{sec})^{0.3}$. (b) Voltage vs t in $s = 0$ for different values of β_ν and ν. (c) Voltage vs s at time $t = 12$ sec for different values of β_ν and ν. The parameter values used for simulations correspond to realistic dendritic parameters as in Ref. [54]: $c_M = 1$ mF/cm^2, $r_M = 3000\ \Omega\,\text{cm}^2$, $r_L = 100\ \Omega\,\text{cm}$, and $R_0 = 10^{-4}$ cm. The initial condition is given by (36).

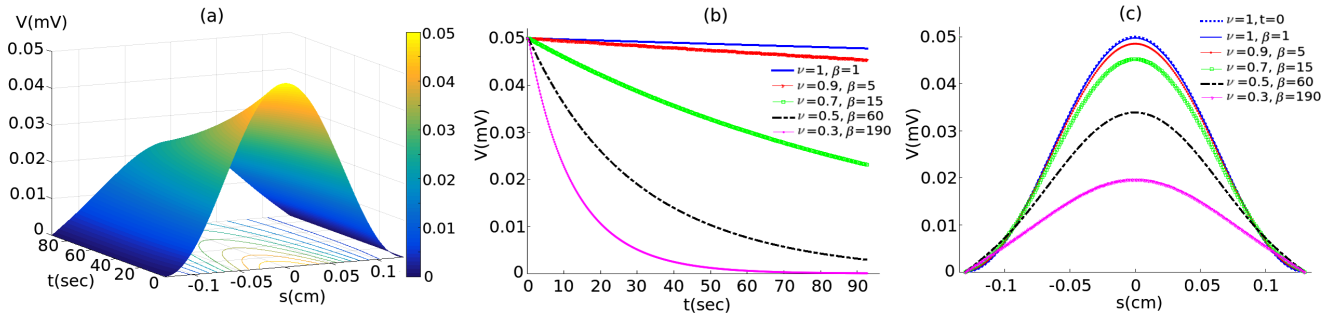

FIG. 4. (a) Voltage for the cylindrical cable for $\nu = 0.7$ and $\beta_{0.7} = 15$ (sec)$^{0.3}$. (b) Voltage vs t in $s = 0$ for different values of β_ν and ν. (c) Voltage vs s at time $t = 12$ sec for different values of β_ν and ν. The parameter values used for simulations correspond to realistic dendritic parameters as in Ref. [54]: $c_M = 1$ mF/cm^2, $r_M = 3000\ \Omega\,\text{cm}^2$, $r_L = 100\ \Omega\,\text{cm}$, and $R_0 = 10^{-4}$ cm. The initial condition is given by (36).

IV. CYLINDRICAL CABLE WITH CONSTANT RADIUS

When the sectional area is a constant, that is, $R(s) = R_0 =$ const, Eq. (15) does not depend on the curvature or on the torsion of the cable. Indeed, in this case Eq. (19) becomes

$$\frac{\partial V(s,t)}{\partial t} = \beta_\nu D_{\nu t}\left(\frac{R_0}{2c_M r_L}\frac{\partial^2 V(s,t)}{\partial s^2} - \frac{V(s,t)}{r_M c_M}\right), \quad (34)$$

which is equivalent to the fractional cable equation for a straight cylindrical cable (1). However, observe that Eq. (34) depends on the arc length parameter (3) instead of the laboratory frame coordinate. This shows that the natural variables for the voltage are given by geometric quantities of the cable. For these geometries, in the finite cable case, the solution of Eq. (34) is given by

$$V(s,t) = \sum_{n\geqslant 0} b_n E_{\nu,1}\left[-\beta_\nu\left(\frac{n\pi R_0}{2c_M r_L l} + \frac{1}{r_M c_M}\right)t^\nu\right]\cos n\pi\frac{s}{l}, \quad (35)$$

where l is the length of the cable and $E_{\nu,\Lambda}(z)$ is the Mittag-Leffler function (28).

Figure 3 shows the fractional cable equation solution for a cylindrical cable for different ν and β_ν values and the initial condition

$$V(s,0) = A\left[1 + \cos\left(\frac{s\pi}{l}\right)\right], \quad (36)$$

where $A = 0.05$ mV cm$^{1/2}$ and $l = 0.13$ cm. In this figure we can see that the voltage decreases when β_ν increases and ν decreases. Then anomalous diffusion implies that voltage decreases.

Obtaining an exact solution of Eq. (34) is a difficult task for an arbitrary initial condition. Thus, in order to study this case we employ a numerical method. For integer derivatives, spatial and temporal, we use a second-order finite-differences method. Moreover, for the temporal fractional derivatives we use a second-order scheme taken from the fractional integration toolbox [61]. The mesh size is chosen as follows. We begin with 1024 points along the s axis and 100 points at the time. These numbers increase until the difference between two successive solutions is almost null. The number of spatial and temporal points used in the simulations are shown in Table I. The system is solved using the Gauss-Seidel iterative method, with a tolerance of 10^{-10}. In addition, we impose the Neumann boundary conditions [59]

$$\frac{\partial V(s_0,t)}{\partial s} = \frac{\partial V(s_{n_s},t)}{\partial s} = 0. \quad (37)$$

Figure 4 shows the numerical solution of Eq. (34) for a cylindrical cable for different ν and β_ν values and the initial condition (36). This figure shows that the numerical solution is close to the analytical solution.

A more realistic initial condition is given by the function

$$V(s,0) = \frac{A}{\sqrt{2\pi\sigma}}e^{-s^2/2\sigma^2}, \quad (38)$$

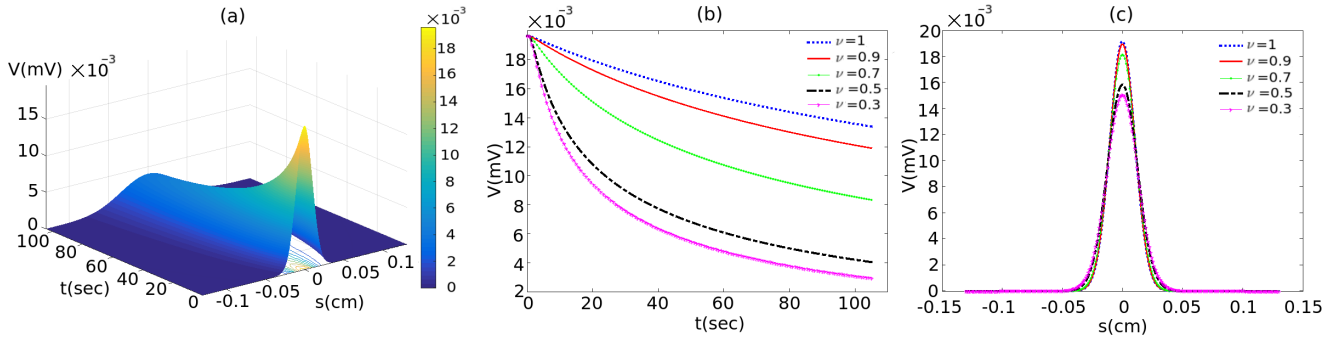

FIG. 5. (a) Voltage for the cylindrical cable for $\nu = 0.5$ and $\beta_{0.5} = 16$ (sec)$^{0.5}$. (b) Voltage vs t in $s = 0$ for different values of β_ν and ν. (c) Voltage vs s at time $t = 7$ sec for different values of β_ν and ν. The parameter values used for simulations correspond to realistic dendritic parameters as in Ref. [54]: $c_M = 1$ mF/cm^2, $r_M = 3000\ \Omega\,\text{cm}^2$, $r_L = 100\ \Omega\,\text{cm}$, and $R_0 = 10^{-4}$ cm. The initial condition is given by (38).

TABLE II. Numerical values of ν and β_ν.

ν	β_ν
1	1
0.9	1.5 $(\text{sec})^{0.1}$
0.7	4 $(\text{sec})^{0.3}$
0.5	16 $(\text{sec})^{0.5}$
0.3	37 $(\text{sec})^{0.7}$

where $A = 0.00128\ \text{mV cm}^{1/2}$ and $\sigma = 0.004$ cm. Figure 5 shows the numerical solution of Eq. (34) for different ν and β_ν values and the initial condition (38). The numerical values of ν and β_ν used in this simulation are shown in Table II.

Notice that both the exact and numerical solutions of Eq. (34) provide a voltage that decreases when β_ν increases and ν decreases. Thus anomalous diffusion implies that voltage decreases. It is worth mentioning that some experimental studies show that in brain tumors there is anomalous diffusion [19–21]. In addition, in different neurodegenerative diseases disrupted axonal transport is reported [24–26]. In these cases, the fractional cable equation implies that the voltage decreases.

In the next section we will study Eq. (19) with nonconstant radius.

V. CABLES WITH SWELLINGS

It can be shown that when a cable has vanished curvature and the cable radius is given by

$$R(s) = R_0(1 + \alpha_1 \sin \alpha_2 s) \tag{39}$$

or

$$R(s) = R_0(1 + \alpha_1 \sin^2 \alpha_2 s), \tag{40}$$

the spatial equation (24) is similar to the spatial equation for the straight cylindrical cable. For this reason, the voltage in a cable with radius (39) or (40) is similar to the voltage in the straight cylindrical cable [56]. Hence, in the fractional case, when a cable has vanished curvature and the radius is given by (39) or (40) the voltage will be similar to voltage (35).

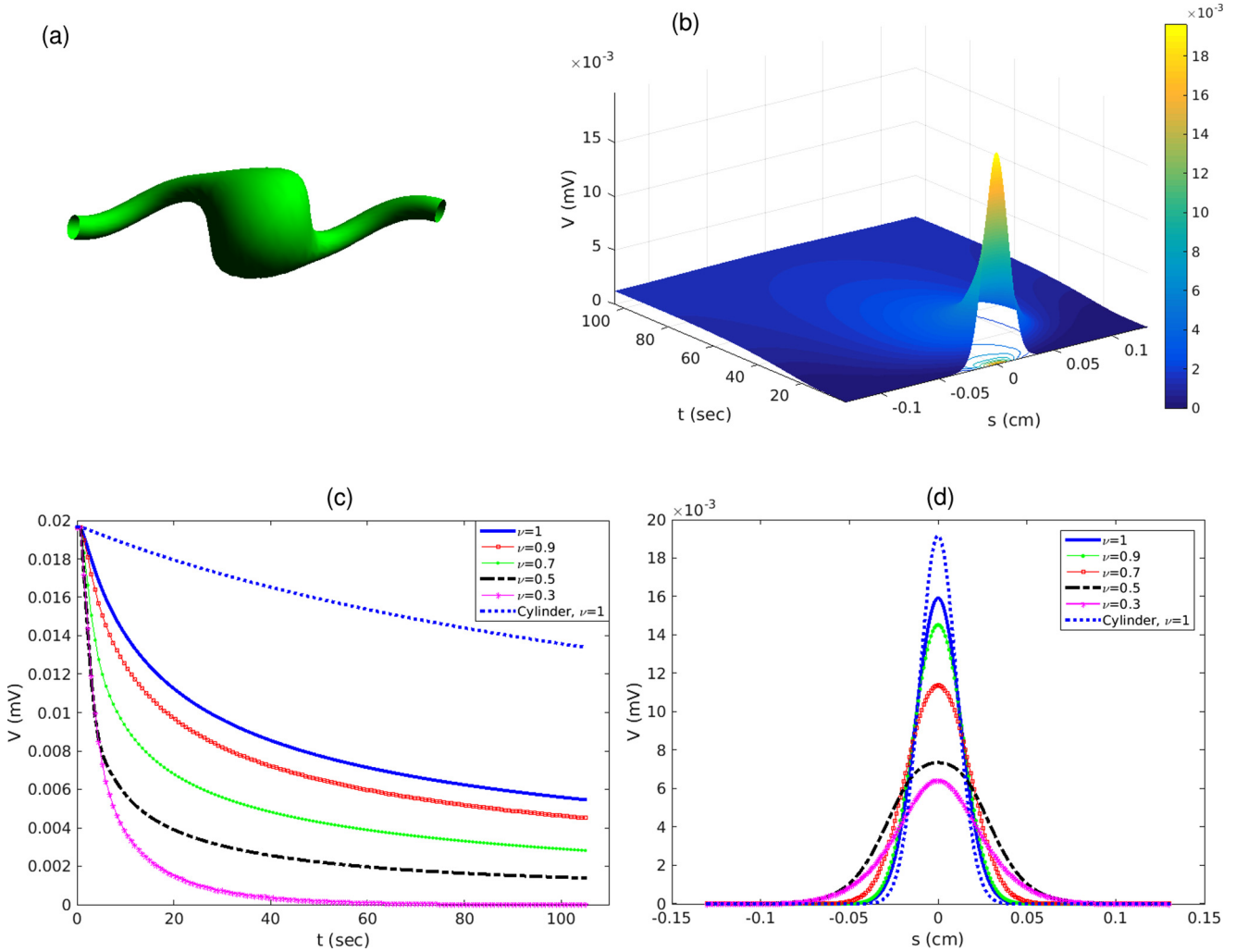

FIG. 6. (a) Cable with the geometry in Eq. (42). (b) Voltage for the cable with the radius (42), $\nu = 0.5$, and $\beta_{0.5} = 16\ (\text{sec})^{0.5}$. (c) Voltage vs t in $s = 0$ for different values of β_ν and ν. (d) Voltage vs s at time $t = 7$ sec for different values of β_ν and ν. The parameter values used for simulations correspond to realistic dendritic parameters as in Ref. [54]: $c_M = 1\ \text{mF/cm}^2$, $r_M = 3000\ \Omega\,\text{cm}^2$, $r_L = 100\ \Omega\,\text{cm}$, $R_0 = 10^{-4}$ cm, $\alpha_1 = 10$, $\alpha_2 = 0.11\ \text{cm}^{-2}$, and $\alpha_3 = 0$ cm. The initial condition is given by (38).

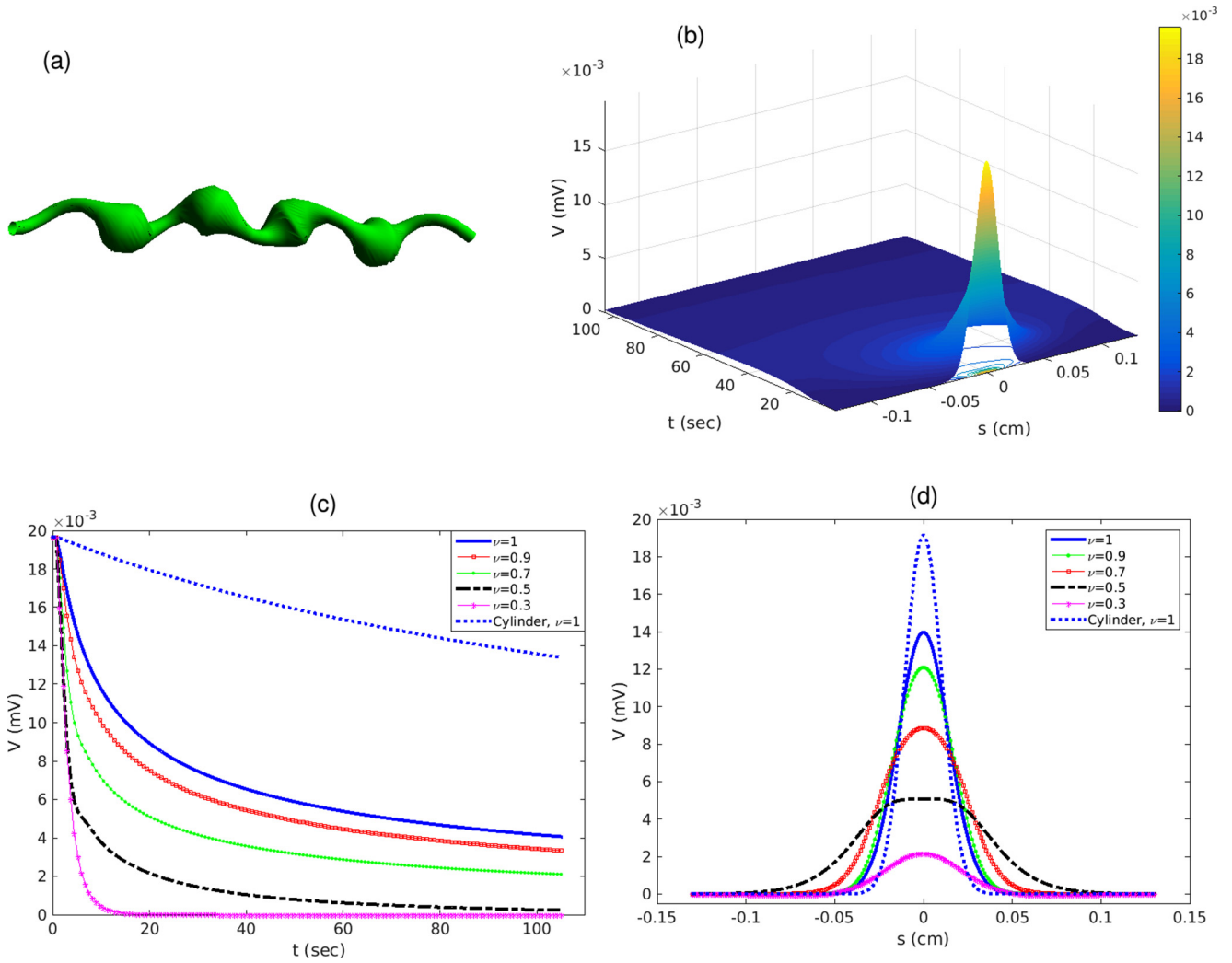

FIG. 7. (a) Cable with the geometry in Eq. (43). (b) Voltage for the cable with a Gaussian train swelling, radius (43), $\nu = 0.5$, and $\beta_{0.5} = 16$ (sec)$^{0.5}$. (c) Voltage vs t in $s = 0$ for different values of β_ν and ν. (d) Voltage vs s at time $t = 7$ sec for different values of β_ν and ν. The parameter values used for simulations correspond to realistic dendritic parameters as in Ref. [54]: $c_M = 1\text{mF/cm}^2$, $r_M = 3000\ \Omega\,\text{cm}^2$, $r_L = 100\ \Omega\,\text{cm}$, $R_0 = 10^{-4}$ cm, $\alpha_1 = 10$, $\alpha_2 = 0.11\ \text{cm}^{-2}$, and $\alpha_3 = 0.06$ cm. The initial condition is given by (38).

A. Circular cross section

The cable equation (19) is hard to solve for a general cable geometry. However, for some cases this equation can be simplified. For instance, when the cable has a circular cross section, namely, when $R(\theta,s) = R(s)$, Eq. (19) does not depend on the torsion of the cable τ and becomes

$$\frac{\partial V(s,t)}{\partial t} = \beta_\nu D_{\nu t}\left(\frac{\pi\frac{\partial}{\partial s}\left(R^2(s)\frac{\partial V(s,t)}{\partial s}\right)}{r_L c_M R(s)\int_0^{2\pi} d\theta\sqrt{[1-\kappa(s)R(s)\cos\theta]^2+\left(\frac{dR(s)}{ds}\right)^2}} - \frac{V(s,t)}{r_M c_M}\right). \tag{41}$$

In the following sections we will study cables that model axons with swellings.

B. Cable with Gaussian swelling

In different neurodegenerative diseases, focal axonal swellings are found such as in Fig. 6(a) (see, for example, [38]). This geometry can be modeled with a cable with radius

$$R(s) = R_0(1+\alpha_1 e^{-\alpha_2(s-\alpha_3)^2}). \tag{42}$$

For this cable geometry, the initial condition is given by (38) and the numerical solution of Eq. (41) can be seen in Figs. 6(b)–6(d). In these figures we can observe that the voltage decreases faster than the voltage of the cylindrical cable. In addition, notice that for this cable geometry when β_ν increases and ν decreases the voltage of the cable decreases faster than when $\beta_1 = 1$ and $\nu = 1$. Then, in an axon with a swelling and anomalous diffusion the voltage strongly decreases.

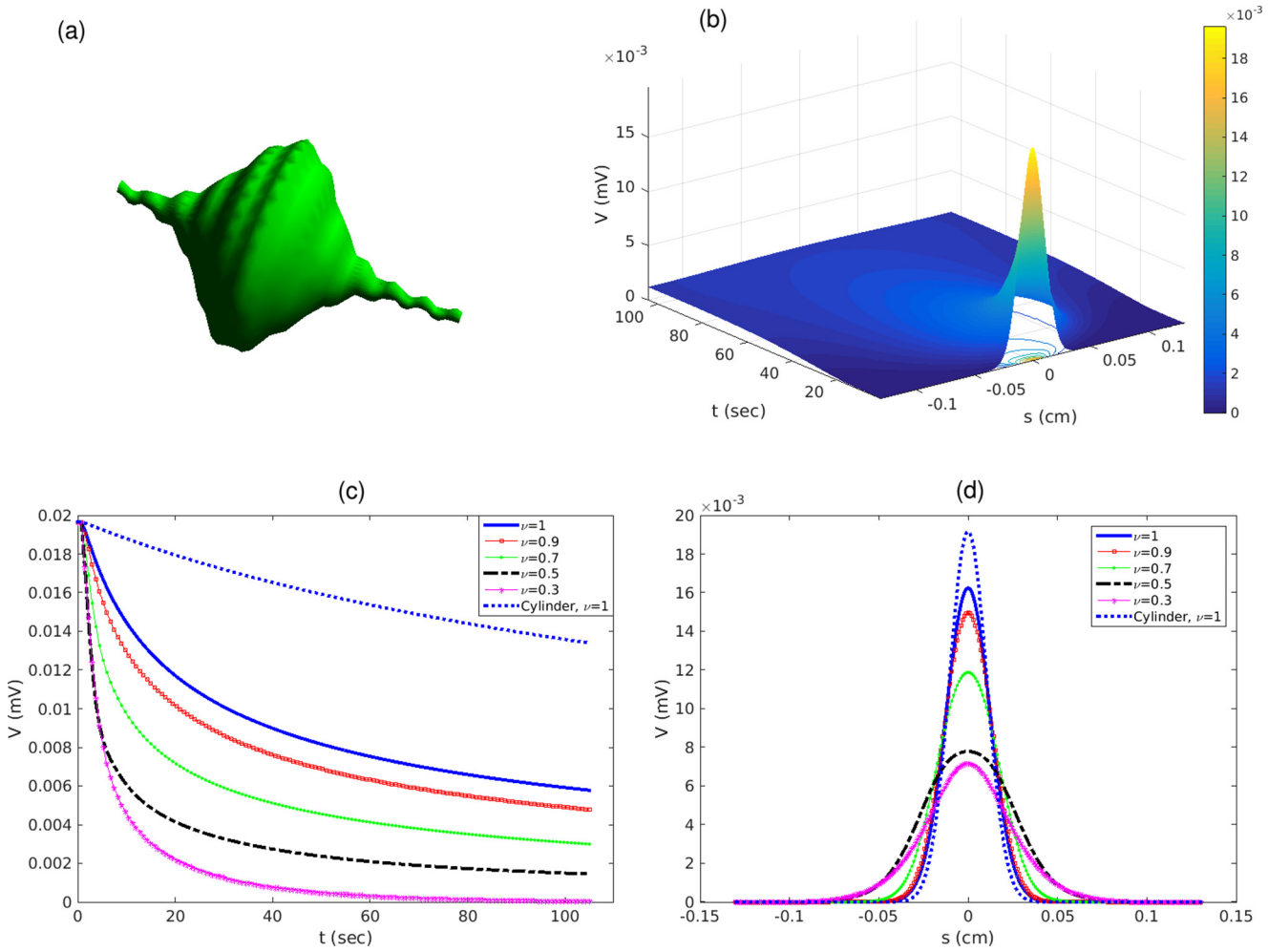

FIG. 8. (a) Cable with the geometry in Eq. (44). (b) Voltage for the cable with the radius (44), $\nu = 0.5$, and $\beta_{0.5} = 16$ (sec)$^{0.5}$. (c) Voltage vs t in $s = 0$ for different values of β_ν and ν. (d) Voltage vs s at time $t = 7$ sec for different values of β_ν and ν. The parameter values used for simulations correspond to realistic dendritic parameters as in Ref. [54]: $c_M = 1$ mF/cm^2, $r_M = 3000\ \Omega\,\text{cm}^2$, $r_L = 100\ \Omega\,\text{cm}$, $R_0 = 10^{-4}$ cm, $\alpha_1 = 10$, $\alpha_2 = 0.11$ cm^{-2}, $\alpha_3 = 0$ cm, $\alpha_4 = 10$, and $\alpha_5 = 0.11$ cm^{-1}. The initial condition is given by (38).

C. Cable with Gaussian swellings

In this section we study the numerical solution for Eq. (41) for a cable with the radius

$$R(s) = R_0(1 + \alpha_1 e^{-\alpha_2 s^2} + \alpha_1 e^{-\alpha_2(s-\alpha_3)^2} + \alpha_1 e^{-\alpha_2(s-2\alpha_3)^2} + \alpha_1 e^{-\alpha_2(s-3\alpha_3)^2}) \quad (43)$$

and with the initial condition (38). A cable with this geometry can be seen in Fig. 7(a). It is worth mentioning that axons with this geometry have been reported in different studies [48]. The numerical solution of Eq. (41) for this cable radius can be observed in Figs. 7(b)–7(d). In this case the voltage decreases faster than the voltage of the cylindrical cable. Moreover, when β_ν increases and ν decreases, the voltage decreases faster than nonfractional voltage ($\beta_1 = \nu = 1$). In addition, we can see that the voltage in a cable with this geometry decreases faster than the voltage in a cable with the geometry in Eq. (42).

D. Amorphous swelling

A more realistic model for an axon with swelling is given by Fig. 8(a). This geometry can be described by a cable with an amorphous swelling with radius

$$R(\theta, s) = R_0(1 + \alpha_1 e^{-\alpha_2(s-\alpha_3)^2} + \alpha_4 \sin\theta \cos\alpha_5 s). \quad (44)$$

The numerical solution of the voltage for this cable can be seen in Figs. 8(b)–8(d). This voltage is different from the voltage for the cable with the radius (42). Thus geometric inhomogeneities affect the voltage propagation in a cable.

VI. SUMMARY

In different neurodegenerative diseases such as multiple sclerosis, Alzheimer's disease, and Parkinson's disease, abnormal accumulations of proteins and organelles are reported that disrupt axonal transport. In addition, recently different experimental studies have found anomalous diffusion in brain tissues. Notably, this diffusion is expressed through fractional calculus. Another hallmark of some neurodegenerative diseases is given by axonal discrete swellings along the axons.

In order to study the voltage propagation in a cable with both of these hallmarks of the neurodegenerative diseases, we proposed a fractional cable equation with nontrivial geometry. This equation depends on geometric quantities such as the

curvature and torsion of the cable, as well as the fractional parameters β_ν and ν. It is worth mentioning that the parameter β_ν depends on ν. In this respect, we showed that with regard to modeling a system where the voltage decreases, we should suppose that β_ν increases when ν decreases. Furthermore, in this cable equation the strongest fractional effect is obtained when ν is close to zero.

For a straight cylinder with a constant radius we showed that the voltage decreases when the fractional effect increases. Notice that in this case the cable does not have swellings. Then, if there is an abnormal accumulation of proteins and organelles in an axon, the diffusion can be hindered and become anomalous. In this case our results suggest that the voltage decreases in axons. Indeed, when the fractional effect is strong, the voltage may be blocked.

In addition, cables with swellings and anomalous diffusion were studied. Regarding this, we studied cable geometries similar to some axons reported in the literature. For all these cable geometries, we found that when the fractional effect increases, the voltage decreases. Furthermore, we found that the voltage dramatically decreases when the cable has a big swelling or has many swellings. These results also suggested that in axons with swellings and abnormal accumulations of proteins and organelles the voltage decreases and may be blocked.

How axonal transport defects and deformed geometry of axons are related each other is an important problem. In order to study this problem, in our model the geometric quantities of the cable should be related to the parameters ν and β_ν. Future work should study the above problem and the active case, where nonlinear interactions play an important role.

ACKNOWLEDGMENTS

This work was supported in part by CONACyT-SEP CB 2012-180111-F (J.M.R.). We are grateful to referees for providing valuable comments.

[1] I. L. Pykett, NMR imaging in medicine, Sci. Am. **246**, 78 (1986).

[2] I. L. Pikett, J. H. Newhouse, F. S. Buonanno, T. J. Brady, M. R. Goldman, J. P. Kistler, and G. M. Pohost, Principles of nuclear magnetic resonance imaging, Radiology **143**, 157 (1981).

[3] J.-D. Tournier, S. Mori, and A. Leemans, Diffusion tensor imaging and beyond, Magn. Reson. Med. **65**, 1532 (2011).

[4] C. Beaulieu, The basis of anisotropic water diffusion in the nervous system—A technical review, NMR Biomed. **15**, 435 (2002).

[5] J. Goveas, L. O' Dwyer, M. Mascalchi, M. Cosottini, S. Diciotti, S. De Santis, L. Passamonti, C. Tessa, N. Toschi, and M. Giannelli, Diffusion-MRI in neurodegenerative disorders, Magn. Reson. Imaging **33**, 853 (2015).

[6] S. K. Song, S. W. Sun, M. J. Ramsbottom, C. Chang, J. Russell, and A. H. Cross, Dysmyelination revealed through MRI as increased radial (but unchanged axial) diffusion of water, NeuroImage **17**, 1429 (2002).

[7] D. J. Werring, C. A. Clark, G. J. Barker, A. J. Thompson, and D. H. Miller, Diffusion tensor imaging of lesions and normal-appearing white matter in multiple sclerosis, Neurology **52**, 1626 (1999).

[8] M. Filippi, M. Cercignani, M. Inglese, M. A. Horsfield, and G. Comi, Diffusion tensor magnetic resonance imaging in multiple sclerosis, Neurology **56**, 304 (2001).

[9] H. D. Rosas, D. S. Tuch, N. D. Hevelone, A. K. Zaleta, M. Vangel, S. M. Hersch, and D. H. Salat, Diffusion tensor imaging in presymptomatic and early Huntington's disease: Selective white matter pathology and its relationship to clinical measures, Movement Disorders **21**, 1317 (2006).

[10] S. J. Choi, K. O. Lim, I. Monteiro, and B. Reisberg, Diffusion tensor imaging of frontal white matter microstructure in early Alzheimer's disease: A preliminary study, J. Geriatric Psych. Neur. **18**, 12 (2005).

[11] N. H. Stricker, B. C. Schweinsburg, L. Delano-Woodd, C. E. Wierengad, K. J. Bangen, K. Y. Haaland, L. R. Frank, D. P. Salmon, and M. W. Bondi, Decreased white matter integrity in late-myelinating fiber pathways in Alzheimer's disease supports retrogenesis, NeuroImage **45**, 10 (2009).

[12] M. P. Laakso, K. Partanen, P. Riekkinen, M. Lehtovirta, E. L. Helkala, M. Hallikainen, T. Hanninen, P. Vainio, and H. Soininen, Hippocampal volumes in Alzheimer's disease, Parkinson's disease with and without dementia, and in vascular dementia: An MRI study, Neurology **46**, 678 (1996).

[13] Y. Bai, Y. Lin, J. Tian, D. Shi, J. Cheng, E. M. Haacke, X. Hong, B. Ma, J. Zhou, and M. Wang, Grading of gliomas by using monoexponential, biexponential, and stretched exponential diffusion-weighted MR imaging and diffusion kurtosis MR imaging, Radiology **278**, 496 (2016).

[14] M. M. Karaman, Y. Sui, H. Wang, R. L. Magin, Y. Li, and X. J. Zhou, Differentiating low- and high-grade pediatric brain tumors using a continuous-time random-walk diffusion model at high b-values, Magn. Reson. Med. **76**, 1149 (2016).

[15] B. Xu, L. Su, Z. Wang, Y. Fan, G. Gong, W. Zhu, P. Gao, and J.-H. Gao, Anomalous diffusion in cerebral glioma assessed using a fractional motion model, Magn. Reson. Med. (2017), doi:10.1002/mrm.26581.

[16] R. L. Magin, O. Abdullah, D. Baleanu, and X. J. Zhoua, Anomalous diffusion expressed through fractional order differential operators in the Bloch-Torrey equation, J. Magn. Reson. **190**, 255 (2008).

[17] K. M. Bennett, K. M. Schmainda, R. T. Bennett, D. B. Rowe, H. Lu, and J. S. Hyde, Characterization of continuously distributed cortical water diffusion rates with a stretched-exponential model, Magn. Reson. Med. **50**, 727 (2003).

[18] K. M. Bennett, J. S. Hyde, and K. M. Schmainda, Water diffusion heterogeneity index in the human brain is insensitive to the orientation of applied magnetic field gradients, Magn. Reson. Med. **56**, 235 (2006).

[19] B. Xu, L. Su, Z. Wang, Y. Fan, G. Gong, W. Zhu, P. Gao, and J.-H. Gao, Anomalous diffusion in cerebral glioma assessed using a fractional motion model, Magn. Reson. Med. (to be published).

[20] M. M. Karaman, H. Wang, Y. Sui, H. H. Engelhard, Y. Li, and X. J. Zhou, A fractional motion diffusion model for grading pediatric brain tumors, NeuroImage: Clinical **12**, 707 (2016).

[21] X.-J. Zhou, Q. Gao, O. Abdullah, and R. L. Magin, Studies of anomalous diffusion in the human brain using fractional order calculus, Magn. Reson. Med. **63**, 562 (2010).

[22] F. Santamaria, S. Wils, E. De Schutter, and G. J. Augustine, Anomalous diffusion in Purkinje cell dendrites caused by spines, Neuron **52**, 635 (2006).
[23] S. Qin, F. Liu, I. W. Turner, Q. Yu, Q. Yang, and V. Vegh, Characterization of anomalous relaxation using the time-fractional Bloch equation and multiple echo T_2^*-weighted magnetic resonance imaging at 7 T, Magn. Reson. Med. **77**, 1485 (2017).
[24] E. Chevalier-Larsen and E. L. F. Holzbaur, Axonal transport and neurodegenerative disease, Biochim. Biophys. Acta **1762**, 1094 (2006).
[25] K. J. De Vos, A. J. Grierson, S. Ackerley, and C. C. J. Miller, Role of axonal transport in neurodegenerative diseases, Annu. Rev. Neurosci. **31**, 151 (2008).
[26] S. Millecamps and J.-P. Julien, Axonal transport deficits and neurodegenerative diseases, Nat. Rev. Neurosci. **14**, 161 (2013).
[27] R. Metzler and J. Klafter, The random walk's guide to anomalous diffusion: A fractional dynamics approach, Phys. Rep. **339**, 1 (2000).
[28] D. S. Novikov, E. Fieremans, J. H. Jensen, and J. A. Helpern, Random walks with barriers, Nat. Phys. **7**, 508 (2011).
[29] M. Palombo, A. Gabrielli, V. D. P. Servedio, G. Ruocco, and S. Capuani, Structural disorder and anomalous diffusion in random packing of spheres, Sci. Rep. **3**, 2631 (2013).
[30] J. M. Haugh, Analysis of reaction-diffusion systems with anomalous subdiffusion, Biophys. J. **97**, 435 (2009).
[31] M. J. Saxon, A biological interpretation of transient anomalous subdiffusion. I. Qualitative model, Biophys. J. **92**, 1178 (2007).
[32] M. Weiss, M. Elsner, F. Kartberg, and T. Nilsson, Anomalous subdiffusion is a measure for cytoplasmic crowding in living cells, Biophys. J. **87**, 3518 (2004).
[33] M. J. Saxon, Anomalous subdiffusion in fluorescence photobleaching recovery: A Monte Carlo study, Biophys. J. **81**, 2226 (2001).
[34] B. I. Henry, T. A. M. Langlands, and S. L. Wearne, Fractional Cable Models for Spiny Neuronal Dendrites, Phys. Rev. Lett. **100**, 128103 (2008).
[35] T. A. M. Langlands, B. I. Henry, and S. L. Wearne, Fractional cable equation models for anomalous electrodiffusion in nerve cells: Infinite domain solutions, J. Math. Biol. **59**, 761 (2009).
[36] L. Debmath and D. Bhatta, *Integral Transforms and Their Applications*, 2nd ed. (Chapman and Hall/CRC Press, New York, 2007).
[37] J. E. Galvin, K. Uryu, V. M.-Y. Lee, and J. Q. Trojanowski, Axon pathology in Parkinson' s disease and Lewy body dementia hippocampus contains α-, β-, and γ-synuclein, Proc. Natl. Acad. Sci. USA **96**, 13450 (1999).
[38] B. D. Trapp, J. Peterson, R. M. Ransohoff, R. Rudick, S. Mörk, and L. Bö, Axonal transection in the lesions of multiple sclerosis, New Engl. J. Med. **338**, 278 (1998).
[39] V. E. Johnson, W. Stewart, and D. H. Smith, Axonal pathology in traumatic brain injury, Exp. Neurol. **246**, 35 (2013).
[40] D. Krstic and I. Knuesel, Deciphering the mechanism underlying late-onset Alzheimer disease, Nat. Rev. Neurol. **9**, 25 (2013).
[41] H. Xie, J. Guan, L. A. Borrelli, J. Xu, A. Serrano-Pozo, and B. J. Bacskai, Mitochondrial alterations near amyloid plaques in an Alzheimer's disease mouse model, J. Neurosci. **33**, 17042 (2013).
[42] H. Budka, G. Costanzi, S. Cristina, A. Leehi, C. Parravicini, R. Trabattoni, and L. Vago, Brain pathology induced by infection with the human immunodeficiency virus (HIV), Acta Neuropathol. **75**, 185 (1987).
[43] F. Gray, F. Chrétien, A. V. Vallat-Decouvelaere, and F. Scaravilli, The changing pattern of HIV neuropathology in the HAART era, J. Neuropathol. Exp. Neurol. **62**, 429 (2003).
[44] M. Kaul, G. A. Garden, and S. A. Lipton, Pathways to neuronal injury and apoptosis in HIV-associated dementia, Nature (London) **410**, 988 (2001).
[45] F. Raja, F. E. Sherriff, C. S. Morris, L. R. Bridges, and M. M. Esiri, Cerebral white matter damage in HIV infection demonstrated using β-amyloid precursor protein immunoreactivity, Acta Neuropathol. **93**, 184 (1997).
[46] R. Ellis, D. Langford, and E. Masliah, HIV and antiretroviral therapy in therain: Neuronal injury and repair, Nat. Rev. Neurosci. **8**, 33 (2007).
[47] M. H. Magdesian, F. S. Sanchez, M. Lopez, P. Thostrup, N. Durisic, W. Belkaid, D. Liazoghli, P. Grütter, and D. R. Colman, Atomic force microscopy reveals important differences in axonal resistance to injury, Biophys. J. **103**, 405 (2012).
[48] G. M. Shepherd and K. M. Harris, Three-dimensional structure and composition of CA3 → CA1 axons in rat hippocampal slices: Implications for presynaptic connectivity and compartmentalization, J. Neurosci. **18**, 8300 (1998).
[49] H. Anwar, C. J. Roome, H. Nedelescu, W. Chen, B. Kuhn, and E. De Schutter, Dendritic diameters affect the spatial variability of intracellular calcium dynamics in computer models, Front. Cell. Neurosci. **8**, 168 (2014).
[50] P. Vetter, A. Roth, and M. Hausser, Propagation of action potentials in dendrites depends on dendritic morphology, J. Neurophysiol. **85**, 926 (2001).
[51] A. D. Bird and H. Cuntz, Optimal current transfer in dendrites, PLoS Comput. Biol. **12**, e1004897 (2016).
[52] E. R. Kandel, J. H. Schwartz, and T. N. Jessell, *Principles of Neural Science* (McGraw-Hill, New York, 2000).
[53] J. C. Fiala and K. M. Harris, Dendrite structure, in *Dendrites*, edited by G. Stuart, N. Spruston, and M. Häusser (Oxford University Press, Oxford, 1999), p. 1.
[54] R. R. Poznanski, Modelling the electrotonic structure of starburst amacrine cells in the rabbit retina: A functional interpretation of dendritic morphology, Bull. Math. Biol. **54**, 905 (1992).
[55] P. D. Maia, M. A. Hemphill, B. Zehnder, C. Zhang, K. K. Parker, and J. N. Kutz, Diagnostic tools for evaluating the impact of focal axonal swellings arising in neurodegenerative diseases and/or traumatic brain injury, J. Neurosci. Methods **253**, 233 (2015).
[56] E. López-Sánchez and J. M. Romero, Cable equation for general geometry, Phys. Rev. E **95**, 022403 (2017).
[57] M. P. Do Carmo, *Differential Geometry of Curves and Surfaces* (Dover, New York, 2016).
[58] M. Spivak, *A Comprehensive Introduction to Differential Geometry* (Publish or Perish, Houston, 1975), Vol. II.
[59] G. B. Ermentrout and D. H. Terman, *Mathematical Foundation of Neuroscience* (Springer, London, 2010).
[60] P. C. Bressloff, *Waves in Neural Media: From Single Neurons to Neural Fields* (Springer, London, 2014).
[61] T. M. Marinov, N. Ramirez, and F. Santamaria, Fractional integration toolbox, Fract. Calc. Appl. Anal. **16**, 670 (2013).